17th World Conference on Earthquake Engineering, 17WCEE
Sendai, Japan - September 13th to 18th 2020

A SEISMIC MASS DAMPER USING SCRAP TIRE PADS: EXPERIMENT ON MECHANICAL PROPERTY AND ANALYSIS OF CONTROL EFFECT

J. Park[1], K. Shirai[2], M. Kikuchi[3]

[1] *Graduate Student, Graduate School of Engineering, Hokkaido University, jpark@eis.hokudai.ac.jp*
[2] *Associate Professor, Faculty of Engineering, Hokkaido University, shirai.kazutaka@eng.hokudai.ac.jp*
[3] *Professor, Faculty of Engineering, Hokkaido University, mkiku@eng.hokudai.ac.jp*

Abstract

Recent studies have proposed using base isolated systems that incorporate scrap rubber pads composed of waste tires from automobiles in the construction of seismic isolation structures with a low cost and high availability. The mechanical characteristics of rubber pad specimens with different configurations, brands, and layer numbers have been experimentally investigated. More recently, the authors have proposed a seismic mass damper system using scrap tire pads (STPs) made by cutting and dividing used tires. Taking advantage of used tires presents a low-cost and environmentally friendly alternative to conventional systems by using recycling materials. In previous studies, the authors have presented the concept, configurations, advantages, and possibilities of the STP proposed system. In the proposed system, STPs are arranged in a vibration control story at the top of a building. The STPs function as a spring and energy dissipator in the mass damper system when subjected to earthquake motion, as well as a bearing to support the weight of the additional mass of the system. However, past research on the dynamic characteristics of STPs is very limited. With the exception of free vibration tests, dynamic loading tests for STPs have not been performed. Moreover, the dependence of the horizontal shear characteristics of STPs on various loading conditions remain unclear.

In the present study, the mechanical properties of STPs were evaluated, and the control effects of the proposed vibration control system using STPs was examined. This paper presents the dynamic characteristics of STPs through loading tests using four STP specimens made by cutting and layering automobile tires. Biaxial tests (i.e., horizontal dynamic loading under constant vertical pressure) and vertical uniaxial loading tests were performed on the STP specimens. Specimens formed by layering six tire pads were tested under the same loading programs. The test results demonstrate the dependence of the shear characteristics on the number of loading cycles, the loading frequency and amplitude, the surface pressure, and the status of the tires. Furthermore, a seismic response analysis was conducted to demonstrate the damping effect of the proposed system. The analysis was performed under various input motions using a multiple-degree-of-freedom model in which a mass damper story was placed at the top of a building structure. For comparison, the response of the model without the mass damper was also investigated. The results of the numerical analysis with the proposed mass damper system using STPs showed the response control effectiveness compared to the case without the vibration control system.

Keywords: Scrap tire pad (STP); Mass damper system; Seismic response analysis; Vibration control structure

1. Introduction

In recent years, researchers have proposed using rubber pads made by cutting and dividing waste tires, called scrap tire pads (STPs), to fabricate low-cost seismic base isolation systems [1, 2]. More recently, Shirai et al. [3–7] have developed a seismic mass damper system using STPs, conducted loading experiments with STPs, and analyzed the response of linear two-degree-of-freedom (2DOF) models. The aim of their proposed system is to increase damping in buildings while using materials that are economical and sustainable. In the proposed system, STPs manufactured by cutting and laminating used tires are arranged on the damping layer at the top of the building. STPs are expected to provide the horizontal stiffness and damping necessary to obtain a mass damper effect during an earthquake. However, few extensive studies on STPs have been conducted to date, and the dependence of STP behavior on various parameters, including the amplitude and velocity of dynamic loadings and surface pressure effects, have not been addressed.

The aim of this study was to experimentally examine the performance of STPs and numerically assess the control effect of the proposed mass damping system. This paper summarizes the mechanical characteristics of the STPs, including the dependence of the horizontal shear characteristics on the loading amplitude and velocity and the number of repetitive loading cycles obtained from the experiments. An earthquake response analysis was also conducted to demonstrate the damping effect of the proposed system placed at the top of a building using a multiple-degree-of-freedom model under various input motions.

2. Loading test

2.1 STP specimens and test program

In this study, horizontal loading under constant surface pressure and vertical compressive loading was applied to four STP specimens. Four test specimens (T1O, T1N, T2O, and T2N) with different tire use periods and manufacturers were tested. The pads were constructed by stacking rectangular pieces of the tire in a six-layer configuration and superposed on each other so that the back and back sides are paired, and the upper and lower sides are brought into contact with the tread surfaces. All STP specimens were produced and tested in the same manner. The specifications of the specimens are given in Table 1, and photographs of the specimens are shown in Fig. 1.

Table 1 – Properties of scrap tire pad specimens

Specimen	T1O	T1N	T2O	T2N
Type	195.65R 15			
Manufacturer	Manufacturer 1		Manufacturer 2	
Status	Used	New	Used	New
Estimated mileage	5000–8000 km	0	5000–8000 km	0
Planar dimension	200 mm × 200 mm (width 100 mm × length 200 mm × 2 columns)			
Layers	6			
Thickness	69 mm	75 mm	70 mm	80 mm

The loading program of the test is given in Table 2. For each specimen, a total of 23 loading runs were performed with each run conducted under different loading conditions. The investigated loading parameters included the surface pressure, frequency, amplitude, and number of cycles. Run 1 was a vertical loading run to obtain the compressive stiffness characteristics of the specimens. Runs 2–22 were horizontal sinusoidal

wave loading runs under constant vertical pressure. Run 23 was a vertical loading to confirm that the STP was able to withstand compression up to 5 MPa. The same test program was applied to every specimen.

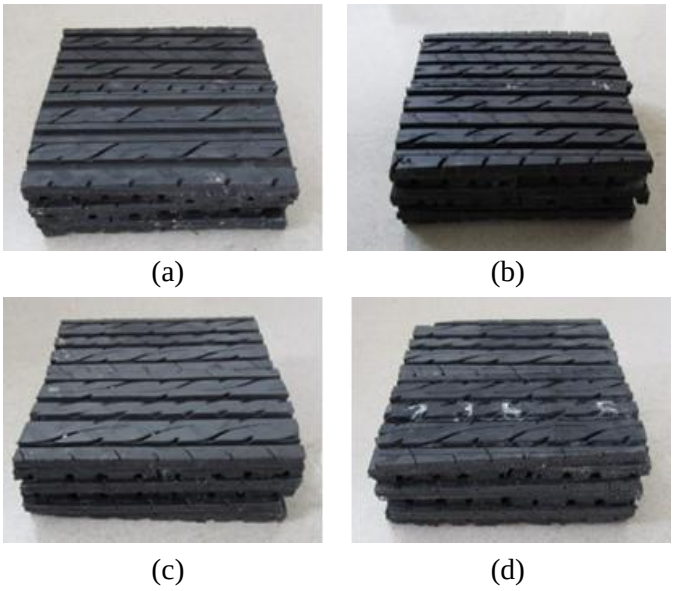

(a) (b)

(c) (d)

Fig. 1 – STP specimens: (a) T1O; (b) T1N; (c) T2O; and (d) T2N

Table 2 – Test program

Run	Vertical	Horizontal			Direction
	Pressure [MPa]	Frequency [Hz]	Amplitude [mm]	Cycles	
1	up to 1.0	-	-	-	Vertical
2/3/4/5	1.0	0.25/1/2/3	5	3	Horizontal + Vertical
6/7/8/9	1.0	0.25/1/2/3	10	3	
10/11/12	1.0	0.25/1/2	20	3	
13/14/15	0.5	0.25	5/10/20	3	
16/17/18	2.0	0.25	5/10/20	3	
19	1.0	0.25	20	30	
20/21/22	1.0	0.25	40/60/80	3	
23	up to 5.0	-	-	-	Vertical

2.2 Vertical compression characteristics

Fig. 2(a) shows the load–displacement relationship in Run 1 under vertical axis loading. The vertical equivalent stiffness K_v was calculated as

$$K_v = (F_1 - F_2)/(\Delta_1 - \Delta_2), \quad (1)$$

where F_1 and F_2 are the maximum and minimum vertical loads, respectively, and Δ_1 and Δ_2 are the corresponding displacements. The equivalent Young's modulus E_v in the vertical direction for the STP specimens were obtained as

$$E_v = K_v t/A, \tag{2}$$

where t is the total thickness of the STP specimen and A is its horizontal area. The values of each of the variables in Eqs. (1) and (2) obtained from Run 1 are given in Table 3 for each specimen. The vertical equivalent stiffness of specimens T1O, T1N, T2O, and T2N in Run 1 was calculated to be K_v = 8.68, 4.49, 9.23, and 5.75 kN/mm, respectively. Additionally, the corresponding Young's moduli E_v were calculated to be E_v =14.92, 8.47, 17.20, and 11.74 N/mm^2, respectively.

In addition, Fig. 2(b) shows the vertical load–displacement curves from Run 23. The results indicate that the STP specimens were able to withstand up to 5 MPa of vertical pressure.

Table 3 – Vertical equivalent stiffness and Young's modulus

Variable	Units	T1O	T1N	T2O	T2N
F_1	kN	38.85	36.96	38.94	34.88
F_2	kN	11.58	13.16	12.05	13.50
Δ_1	mm	30.27	25.15	23.98	16.46
Δ_2	mm	27.13	19.85	21.07	12.74
K_v	kN/mm	8.68	4.49	9.23	5.75
t	mm	68.75	75.5	74.5	81.75
A	mm^2	40000	40000	40000	40000
E_v	N/mm^2	14.92	8.47	17.20	11.74

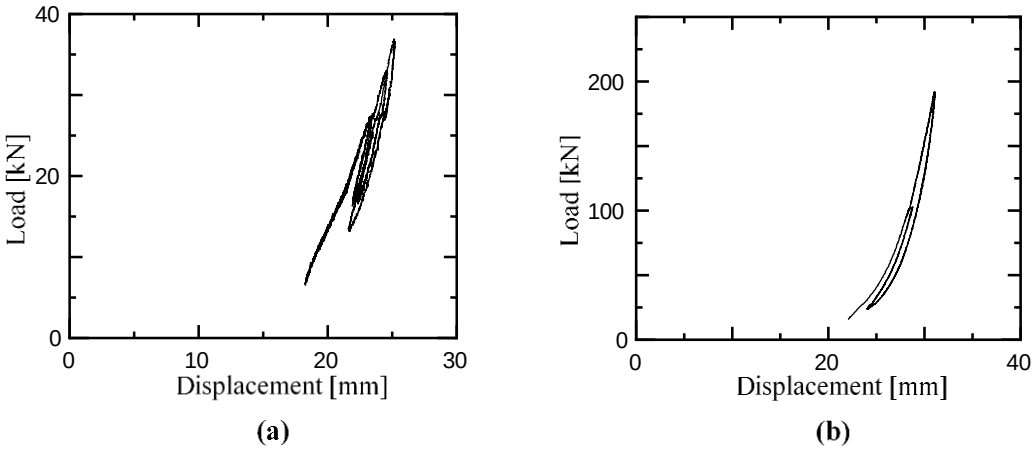

Fig. 2 – Vertical load–displacement curves: (a) surface pressure up to 1 MPa (Run 1, T1N); and (b) surface pressure up to 5 MPa (Run 23, T2O)

2.3 Horizontal shear characteristics

Each STP specimen displayed a thick oval or spindle-shaped hysteresis loop when loading was applied in the horizontal direction, as shown in Fig. 3. This demonstrates that the STP alone has a certain damping performance, which is consistent with findings obtained in past studies [1, 2].

The equivalent stiffness and equivalent viscous damping factor in the horizontal direction were calculated for each run of each specimen, and their dependence on four test parameters—the number of repeated loading cycles, the loading frequency and amplitude, and the surface pressure—was examined, as

described in detail below. The results of the loading tests indicate that all of the STP specimens showed similar tendencies in their dependence on these parameters, although there were small differences depending on the status and manufacturer of the tires.

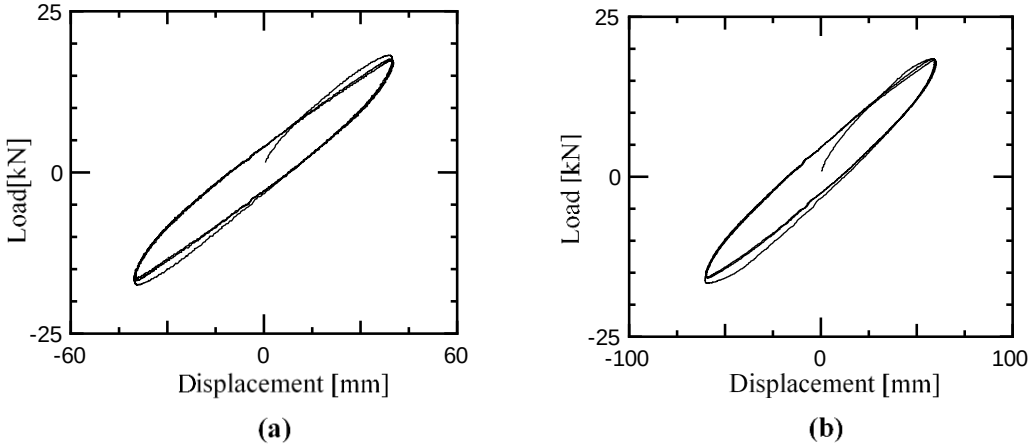

Fig. 3 – Horizontal load–displacement curves: (a) loading displacement of 40 mm (Run 20, T1O); and (b) loading displacement of 60 mm (Run 21, T2N)

2.3.1 Repeated load dependence

From the experimental data of Run 19, which included 30 loading cycles, the shear characteristics were computed after each cycle to observe how they changed with increasing cycle number, as shown in Fig. 4. Both the equivalent stiffness and viscous damping factor changed slightly in the first five cycles; however, the rate of change became smaller in subsequent cycles. In addition, relative to the values in the first cycle, the equivalent stiffness in the 30th cycle decreased by 6.6%, 7.8%, 3.8%, and 4.7% for the T1O, T1N, T2O, and T2N specimens, respectively, and the equivalent viscous damping factor changed by 0.7%, 2.4%, 2.1% and 2.5%, respectively. No failure or damage was observed in the STP specimens during the 30 loading cycles. These results demonstrate that the performance of the equivalent stiffness and the equivalent viscous damping factor was not greatly reduced by repeated loading.

2.3.2 Frequency dependence

Fig. 5 shows the equivalent stiffness and viscous damping factor plotted against the loading frequency for four frequency values (0.25, 1, 2, and 3 Hz). These results were obtained under horizontal loading with a surface pressure of 1.0 MPa, and the equivalent stiffness and damping factor were calculated at the third cycle of a three-cycle loading run. In each of the specimens, the equivalent stiffness increased gradually with increasing frequency; however, the rate of change was not constant and gradually decreased with increasing frequency. Furthermore, as the frequency increased, the equivalent viscous damping factor also increased.

2.3.3 Amplitude dependence

Fig. 6 shows the equivalent stiffness and viscous damping factor plotted against the loading amplitude under horizontal loading with a frequency of 0.25 Hz. For all specimens, larger amplitudes corresponded to lower equivalent stiffness values. Additionally, the equivalent viscous damping factor decreased with increasing amplitude until an amplitude of 40 mm and then increased for amplitudes beyond 60 mm.

2.3.4 Surface pressure dependence

Each specimen showed increasing equivalent stiffness when the surface pressure increased. The equivalent viscous damping factor also increased slightly with increasing surface pressure.

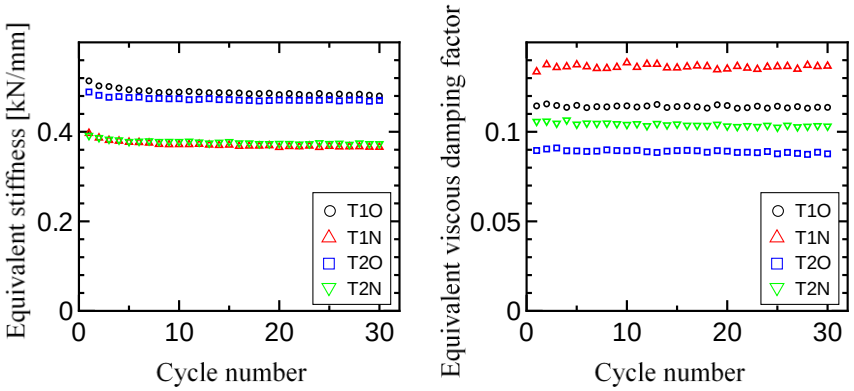

Fig. 4 – Cyclic loading dependence of the horizontal shear characteristics (Run 19)

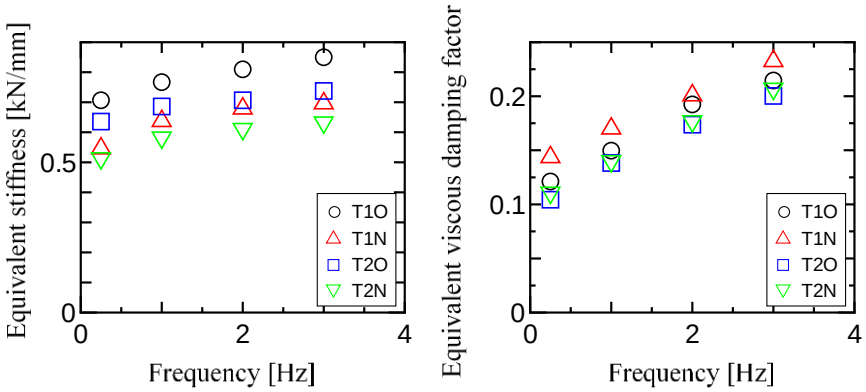

Fig. 5 – Frequency dependence of the horizontal shear characteristics

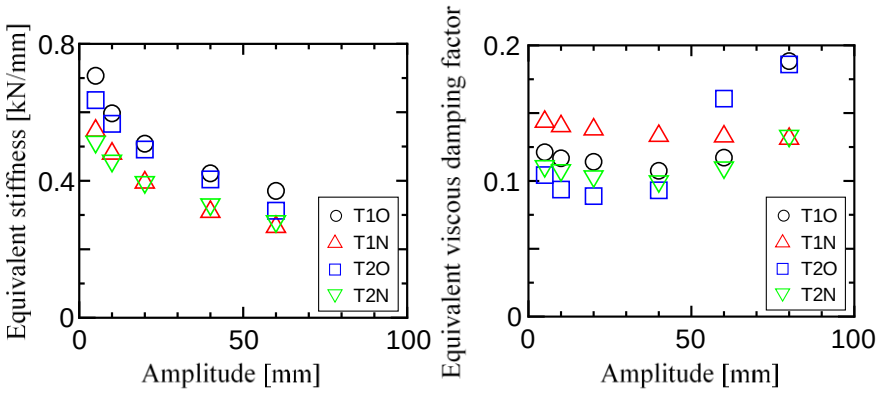

Fig. 6 – Amplitude dependence of the horizontal shear characteristics

3. Earthquake response analysis

3.1 Analysis methods

A fixed base building model (FIX) and building models with sway-rocking motions (SR1 and SR2) were used to perform earthquake response analysis. Fig. 7 shows the analysis models. Trilinear restoring force characteristics (Fig. 8) were given for the main frame of each superstructure, where K_1 is the initial stiffness

and K_2 and K_3 are the tangent stiffness after the cracking and yielding, respectively. The models were developed based on a design example of a 10-story building [8], and the model parameters are given in Table 4. In the models with a mass damper, a mass with a mass ratio of 0.1 was placed at the top of each superstructure. For comparison, the response for models without a mass damper was also investigated. Table 5 gives the specifications of the sway and rocking motions for the SR1 and SR2 models. Based on the loading test results with a frequency of 2 Hz and amplitude of 20 mm, the equivalent stiffness and viscous damping for a single STP unit were set to be 0.56 kN/mm and 0.17, respectively.

The analysis cases are listed in Table 6. Case N represents the case without mass dampers. In Case 1, the lateral stiffness K_d and the damping coefficient C_d for the mass damper story were set to correspond to the elastic natural period without the mass damper. In Cases 2 and 3, K_d and C_d were set to be lower (×0.5 and ×0.25) than those in Case 1. The ratio of C_d to K_d was set based on the results of the loading tests.

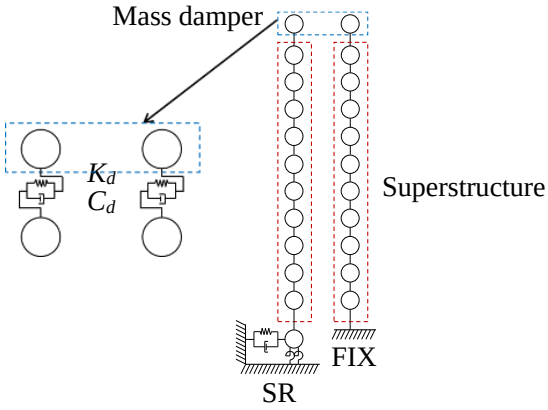

Fig. 7 – Analysis model

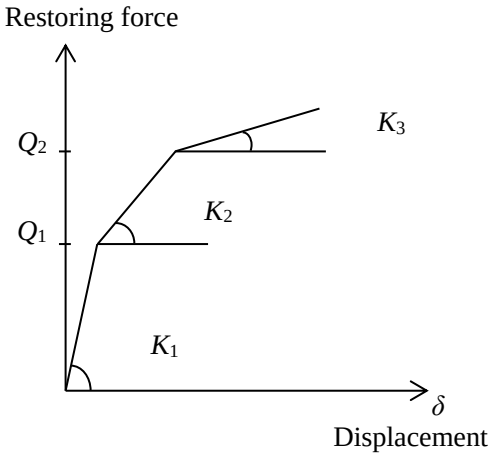

Fig. 8 – Restoring force properties

Table 4 – Model configuration

Floor	Height [m]	Weight [kN]	K_1 [kN/m]	K_2 [kN/m]	K_3 [kN/m]	Q_1 [kN]	Q_2 [kN]
R	-	18780	-	-	-	-	-
10	3.8	17490	5960000	2830000	209000	14100	29700
9	3.8	17470	8330000	3210000	132000	16600	48500
8	3.8	17570	10200000	4440000	314000	17700	57600
7	3.8	17600	11800000	5420000	445000	19000	64400
6	3.8	17840	14000000	6580000	513000	24400	71100
5	3.8	17820	16000000	7760000	599000	24300	75800
4	3.8	17940	18100000	8730000	674000	26400	79900
3	3.8	18910	22200000	15700000	706000	33200	84500
2	4.2	24670	28800000	24800000	623000	28000	93900
1	4.5	59430	38500000	36900000	1460000	40400	99600

Damper	Height [m]	Weight [kN]	K_d [MN/m]	C_d [MN/(m/s)]
FIX	2.9	18609	364.9865784	8.950882259
SR1	2.9	18609	231.7876223	7.133004818
SR2	2.9	18609	204.807543	6.705024529

Table 5 – Specifications of sway and rocking motions

Element	SR1	SR2
Sway stiffness [kN/m]	9550000	7590000
Sway damping [kN·s/m]	294000	625000
Rocking stiffness [kN·m/rad]	1.72×10^{10}	1.14×10^{10}
Rocking damping [kN·m·s/rad]	217000000	230000000

Table 6 – Analytical cases

	Case N	Case 1	Case 2	Case 3
K_d and C_d	No mass damper	×1.0	×0.5	×0.25

As input seismic waves, 10 earthquake observation data were used (1940 El Centro, 1952 Taft, 1968 Hachinohe, 1978 Tohoku, and 1995 Kobe; each for NS and EW direction) [9, 10]. Each input wave was normalized to 0.5 m/s.

For each analysis case, viscous damping (damping factor of 2%, stiffness proportional type) was adopted as the structural damping of the entire system. For the numerical integration, the Newmark-β method ($\beta = 1/4$) was used with a time increment of 0.005 s.

3.2 Analysis results

Fig. 9 shows the maximum response reduction ratio for the main structures in Cases 1–3 averaged over the 10 input seismic motions and normalized with respect to the corresponding ratio in Case N. In all cases, the controlled models (Cases 1–3) showed a significant decrease in the maximum response acceleration compared to the non-controlled model (Case N). In contrast, for the maximum response displacement, Case 1 showed no reduction in response relative to Case N. In Cases 2 and 3, the maximum response displacement was less than that in Case N. This indicates that the earthquake response is effectively reduced by setting the lateral stiffness and damping coefficient for the mass damper story to be smaller than those corresponding to the elastic natural period, in consideration of decreasing the equivalent stiffness of the main frame due to the progress of damage and plasticity.

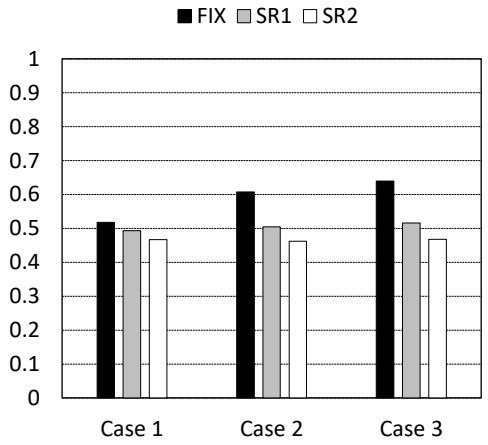

(a) Response reduction ratios for acceleration

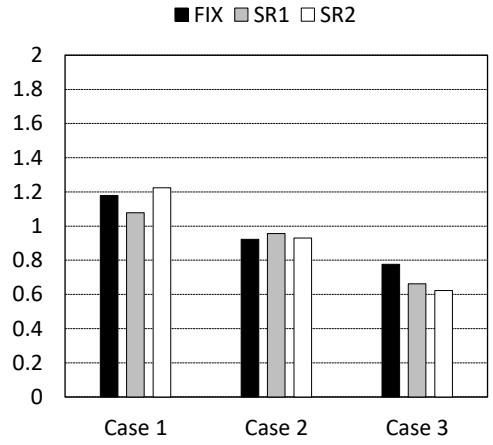

(b) Response reduction ratios for displacement

Fig. 9 – Average response reduction ratios in Cases 1–3 normalized with respect to that in Case N for the peak response values of the main structure

4. Conclusion

In this study, the results of loading experiments of four different STP specimens were analyzed and an earthquake response analysis of models with or without the proposed mass dampers was performed. The following results were obtained.

1) The fundamental mechanical characteristics were determined by performing horizontal dynamic loading tests with constant vertical pressure and quasi-static vertical loading on the four STP specimens.

2) The test results were used to evaluate the dependence of the equivalent stiffness and viscous damping factor of the STP specimens on the number of loading cycles, the loading amplitude and frequency, and the vertical surface pressure.

3) A seismic response analysis was conducted using a 10-story nonlinear building model under fixed-base or sway-rocking motions with or without a mass damper. The results demonstrated that incorporating the proposed system using STPs achieved a response reduction effect.

5. Acknowledgments

We thank Dr. Hideaki Kato and Dr. Masahiro Nakamura of Bridgestone Corporation for conducting the loading tests in this study. We would also like to express our gratitude to the Japan Meteorological Agency and Building Performance Standardization Association for providing the seismic observation data used in the analysis in this study. This study was supported by the Japan Society for the Promotion of Science, KAKENHI Grant number 16K14180.

6. References

[1] Turer A, Özden B (2008): Seismic base isolation using low-cost Scrap Tire Pads (STP), *Materials and Structures*, **41**, 891-908.

[2] Mishra HK, Igarashi A, Matsushima H (2013): Finite element analysis and experimental verification of the scrap tire rubber pad isolator, *Bulletin of Earthquake Engineering*, **11**, 687-707.

[3] Shirai K, Kikuchi M (2015): A proposal of a seismic mass damper system using waste tires appropriate for RC building structures, *Summaries of technical papers of Annual Meeting Architectural Institute of Japan*, C-2, 609-610.

[4] Shirai K, Park J, Kikuchi M (2017): A proposal of a seismic mass damper system using waste tires appropriate for RC building structures Part 2: Methods and results of loading tests on a STP specimen, *Summaries of technical papers of Annual Meeting Architectural Institute of Japan*, B-2, 743-744.

[5] Park J, Shirai K, Kikuchi M (2017): A proposal of a seismic mass damper system using waste tires appropriate for RC building structures Part 3: Analyzing Experimental Data and Earthquake Response Analysis, *Summaries of technical papers of Annual Meeting Architectural Institute of Japan*, B-2, 745-746.

[6] Park J, Shirai K, Kikuchi M (2018): A proposal of a seismic mass damper system using waste tires appropriate for RC building structures Part 4: Experimental Results of Different STP specimens", *Summaries of technical papers of Annual Meeting Architectural Institute of Japan*, B-2, 353-354.

[7] Shirai K, Park J (2020): Use of scrap tire pads in vibration control system for seismic response reduction of buildings, *Bulletin of Earthquake Engineering*.

[8] Architectural Institute of Japan (2007): *Seismic Response Analysis and Design of Buildings Considering Dynamic Soil-Structure Interaction*. AIJ, 2nd edition.

[9] Building Performance Standardization Association. https://www.seinokyo.jp/jsh/top/. Access date: December 10, 2019.

[10] Japan Meteorological Agency. https://www.data.jma.go.jp/svd/eqev/data/kyoshin/jishin/hyogo_nanbu/index.html. Access date: December 10, 2019.

